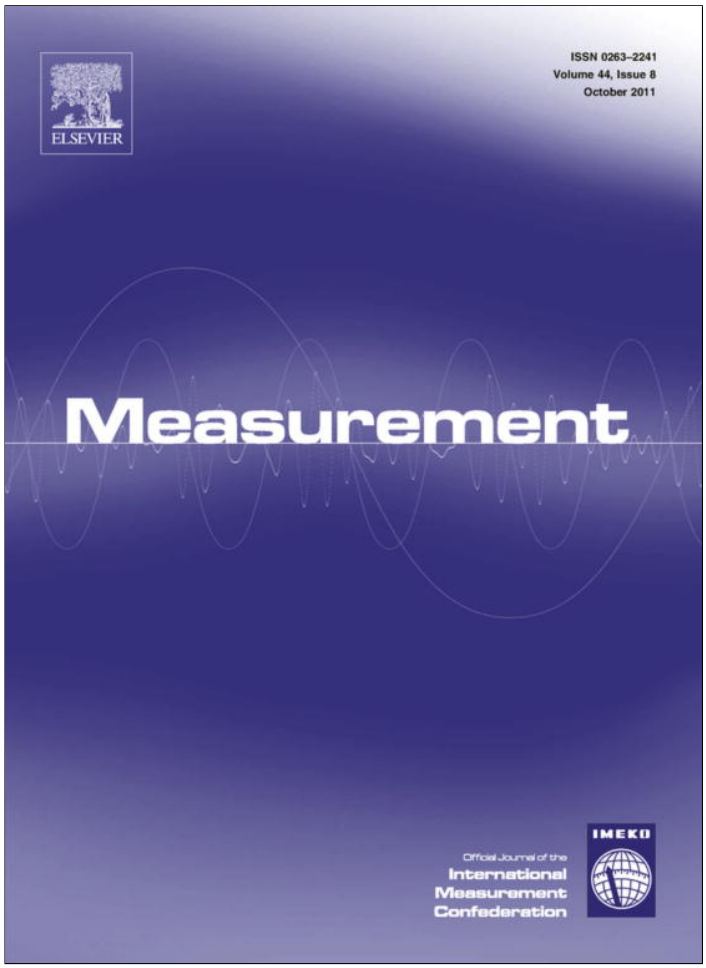

Measurement 44 (2011) 1412–1421

Contents lists available at ScienceDirect

Measurement

journal homepage: www.elsevier.com/locate/measurement

Measurement evaluations of static and low frequency magnetic fields in the near field region

Saba A. Hanna, Yuichi Motai *, Walter Varhue, Steve Titcomb

Virginia Commonwealth University, School of Engineering, 601 West Main Street, PO Box 843072, Richmond, VA 23834-3072, United States

ARTICLE INFO

Article history:
Received 20 April 2010
Received in revised form 15 April 2011
Accepted 12 May 2011
Available online 24 May 2011

Keywords:
Gaussmeter
Very low frequency
Magnetic field measurements
Safe public
Occupational exposure

ABSTRACT

Manmade electromagnetic (EM) field in the low frequency range of the spectrum, from static to 200 kHz has caused interference with electronic equipment and poses a possible public health risk. Typical sources of these EM emissions include television sets, video display terminals (VDT), electric appliances, fluorescent lights, certain medical devices, walk-through and hand-held detectors, radio stations, induction heating, wireless electricity delivered over distance, hybrid cars and transmission lines. Our main goals for writing this paper are, first, to describe taking measurements of the frequencies and magnetic field levels in residential and occupational environments, particularly around cathode ray tube displays, induction heating units, and hybrid cars; and, second, to compare the measurements to the established or recommended limits according to national standards so that engineers and scientists can understand these nontrivial electrical measurements. The field measurements were carried out using different kinds of devices where a brief description of the instruments used is also provided.

1. Introduction

Human exposure to low frequency EM radiation is not a new concern. Our environment has always contained this type of naturally occurring radiation as a result of solar activity, meteorological changes, and biosphere activity. From the beginning of the twentieth century, environmental exposure to manmade electromagnetic fields has been increasing exponentially since the growing demand for electricity, ever-advancing technologies, and changes in social behavior have created more and more artificial sources. Although devices generating EM radiation have become an essential part of our lives due to the numerous applications, there are mounting concerns about the bioeffects that might exist due to exposure to such fields [1,2]. In this paper we evaluate the magnetic fields around cathode ray tube displays since they have been so widely used for many decades. Induction heating units were also evaluated due to the potentially long exposure in an industrial environment. Finally, hybrid cars were studied to better understand the risks associated with the new technology introduced in the vehicles. Previous papers have not reported rigorous magnetic field measurements for any of these case studies.

For over two decades, researchers have investigated the possibility that exposure to low frequency EM waves might lead to potential health hazards. International scientific groups believe that the data are not sufficient to draw the conclusion that EM radiation causes cancer or leads to the disruption of biological systems [3,4]. On the other hand, some health effects have been statistically related to EM exposure [5–12]. Since not all research issues have been settled and reliable results are not forthcoming, continued research will be required before a firm conclusion can be reached.

Generally accepted guidelines have been established by the International Commission on Non-Ionizing Radiation Protection (ICNIRP) [4]. The recommended exposure levels for time-varying magnetic fields with frequency from 1 Hz to 10 MHz in an occupational environment and general public are presented in Tables 1 and 2.

* Corresponding author. Tel.: +1 804 828 1281.
E-mail address: ymotai@vcu.edu (Y. Motai).

0263-2241/$ - see front matter © 2011 Elsevier Ltd. All rights reserved.
doi:10.1016/j.measurement.2011.05.008

Table 1
Reference levels for occupational exposure to time-varying magnetic fields in the range from 1 Hz to 10 MHz (unperturbed RMS values).

Frequency range	B magnetic field density: μT f in Hz	B magnetic field density: mG f in Hz
1–8 Hz	$2 \times 10^5/f^2$	$20 \times 10^5/f^2$
8–25 Hz	$2.5 \times 10^4/f$	$25 \times 10^4/f$
25–300 Hz	1×10^3	1×10^4
300–3 kHz	$3 \times 10^5/f$	$3 \times 10^6/f$
3–10 MHz	1×10^2	1×10^3

Table 2
Reference levels for general public exposure to time-varying magnetic fields in the range from 1 Hz to 10 MHz (unperturbed RMS values).

Frequency range	B magnetic field density: μT f in Hz	B magnetic field density: mG f in Hz
1–8 Hz	$4 \times 10^4/f^2$	$4 \times 10^5/f^2$
8–25 Hz	$5 \times 10^3/f$	$5 \times 10^4/f$
25–400 Hz	2×10^2	2×10^3
400–3 kHz	$8 \times 10^4/f$	$8 \times 10^5/f$
3–10 MHz	27	270

The magnetic field levels specified above by the ICNIRP are frequency dependent, with different levels for public and occupational exposure. These guidelines are intended to prevent negative effects, such as induced currents in cells or nerve stimulations. Several institutions have criticized the guidelines for lacking clear interpretation on exposure safety and long-term exposure to equipment that generates magnetic fields.

These controversial scientific and technical issues pose the need for more research to improve the health risk assessments and the reliability of the measurements. One technique for improving the measurements is to use multiple instruments with different specifications to fully understand the nature of the magnetic fields. This technique includes quantifying the radiation fields with a device that measures the magnetic field components in the VLF–LF band. The measured magnetic field can be any one of the true RMS vector components (B_x, B_y, or b_z), or the resultant ($B_R = \sqrt{B_x^2 + B_y^2 + B_z^2}$) of magnetic fields. The recently introduced IDR-200 was used to measure fields in the VLF–LF band. These measurements were complemented by the IDR-309-T, which was used to measure the static (DC) magnetic field, and the IDR-210, which measured magnetic fields in the bandwidth (BW) range from 20 Hz to 4 kHz. The high precision, resolution, and multiple features of the IDR-200 provide an important tool needed by researchers for taking accurate and complete measurements of magnetic fields from 1 kHz to 200 kHz.

The IDR-200 magnetic field meter has been designed to have a very low frequency (VLF) and low frequency (LF) bandwidth frequency response from 1 kHz to 200 kHz, with a dynamic measurement range from 0.2 to 2000 mG. In the United States, the magnetic field is generally measured in CGS units: Gauss (G), while in most of the rest of the world, it is measured in SI unit: Tesla (T). Since most low frequency bands environmental exposures involve magnetic field intensities that are only a fraction of Tesla or Gauss, the common units used for measurements are either microTesla (μT) or milliGauss (mG) with conversion: 10 mG = 1 μT. The detection circuit utilizes three orthogonal multi-turn copper loops that respond to time-varying magnetic fields. The field measurements are also made available externally through a RS-232 communication port and an analog recorder output.

This paper is organized as follows. Section 2 discusses some of the related work that has been done in the areas of static, super low frequency (SLF), VLF and LF magnetic field measurement. Section 3 briefly discusses the theory of operation of the IDR-200, the operation of the meter including the analog front end, the design approaches, and the SPICE simulation of the analog subsystem [13]. Section 4 discusses the system architecture. Section 5 describes calibration, characterization, and measurements of magnetic fields in the cathode ray tube, induction heating coil, and hybrid car environments.

2. Comparison with other related works in magnetic field measurement

Most of the previous papers described and analyzed the measurement results of the magnetic field level for SLF frequency especially for 50 and 60 Hz generated by power lines and substations. Safigianni and Tsompanidou [2] measured the 50 Hz electric and magnetic field caused by the operation of indoor power distribution substations. In another study, Sekerinska and Dimcev [25] covered the measurements of the magnetic field strength at 60 Hz inside homes, under the transmission lines and around the substation. Sapashe and Ashely [21] presented the measurements of VDT fringing magnetic fields. In his measurement, he used a single axis coil with a basic detector that has limited BW and a relative reading with an error of 10%. Also, the device was not calibrated against any traceable standard. Recently, Motavalli [23] reported the measurement of the magnetic fields inside the hybrid cars. In his report, he missed some important points, especially the discussion of the DC magnetic field created by the power moving to and from a hybrid vehicle's battery. Also, the Trifield AC Gaussmeter used in his testing did not have the feature to measure the DC magnetic field and it was a frequency-weighted unlike the rest of the most commercial Gaussmeters.

This paper examines the measurement of the magnetic field from DC to 200 kHz by using accurate and appropriate devices for each specific band of the frequency spectrum under study. It analyzes clearly and precisely the magnetic field around the VDTs and inside the hybrid cars, an issue poorly and insufficiently addressed in previous papers. The usage of innovative devices during the testing plays a key role in providing highly accurate measurement results.

3. Sensor theory and design

A multi-turn copper coil is used as a field-sensing element in this detector design. According to Faraday's law

of induction, the peak voltage signal, V_{in}, produced by a coil positioned transverse to an incident magnetic field [14] is

$$V_{in} = 2\pi fNAB \quad (1)$$

where N is the number of turns in the coil; B is amplitude of magnetic flux density; A is coil cross-sectional area; f is magnetic field frequency.

A sketch of the induction coil sensor is shown in Fig. 1. A coil of 5 cm^2 in cross-sectional area has been chosen for the convenience of use and resolution of the potential measurement. Further, it is desired to use standard electronic hardware and a maximum voltage amplitude of 6 V for a magnetic flux density of 2000 mG and a frequency of 200 kHz. A design based on these assumptions and goals yields a sensor containing 47 wire turns. The resonance frequency fr for the coil was measured and was found to be equal to 2800 kHz [15]. Therefore, the air coil sensor is operating as a linear inductor over the required BW frequencies.

The analog front-end of the sensor circuitry associated with three-dimensional isotropic probe coils for x, y, z measurements are represented as a block diagram in Fig. 2. The switching signal from each coil is fed into an integrator section that provides a flat frequency response. The output of the integrator is filtered and amplified by a wide band pass filter to ensure that only the desired signals are fed to an AC to DC converter where the DC output is compatible with the 0–5 V range of the analog-to-digital converter. The same signal is also fed to an analog output that is capable to display a sinusoidal and no sinusoidal wave and a comparator to generate a square wave digital signal (0 V or 5 V) compatible with the frequency counter. A more complete discussion of the individual components, which make up the analog front-end design in Fig. 2 have been discussed in an earlier publication [16].

4. System architecture

The analog front-end and the digital components are combined to form the complete measurement system shown in Fig. 3. The analog front-end processes the signal from the coil sensor and generates two outputs. The RMS output from the analog front-end is connected to the input of the 10-bit ADC for further digital signal processing and the square wave output is connected to the frequency counter.

The microcontroller controls the channel selection based on input from the user through the keypad or RS232 port. The variable gain amplifier in the analog front end is controlled by the range selection signals from the microcontroller. The range selection can be set manually or the microcontroller can dynamically select the range based on the measurements from the coil sensor [16].

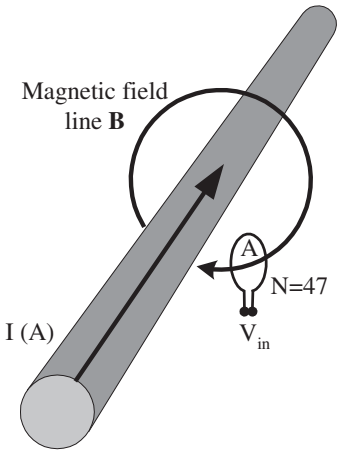

Fig. 1. Air coil loop sensor (r = 1.27 cm) where the number of turns N is equal to 47 #38 Cu is mounted transverse to the magnetic field lines.

5. Magnetic field meter performance

5.1. Calibration procedure

The detector developed shown in Fig. 4 processes the signal from the probe and indicates the RMS value of the magnetic waveform field with an analog output and digital display. The calibration tests for the Gaussmeter are done during the manufacturing process by placing the probe into a varying sinusoidally magnetic field with time of known magnitude and direction produced by a circular Helmholtz coil [16–18]. Characterization of the Gaussmeter IDR-200.

The linearity error over the measured frequency range was less than 3% for the worst case. The formula used to calculate this percentage error is as follows:

$$\%Error = \left(\frac{Measured\ Field\ (RMS) - Theoretical\ Field(RMS)}{Theoretical\ Field(RMS)}\right) * 100 \quad (2)$$

According to the EPA [19], meters with more than 5% error should be considered inaccurate.

All testing for the prototype development was done at a nominal temperature of 25 °C [16]. We expect all the

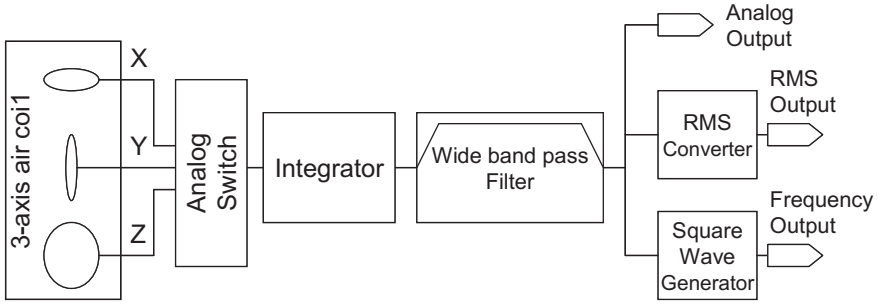

Fig. 2. Basic block diagram for the analog front-end.

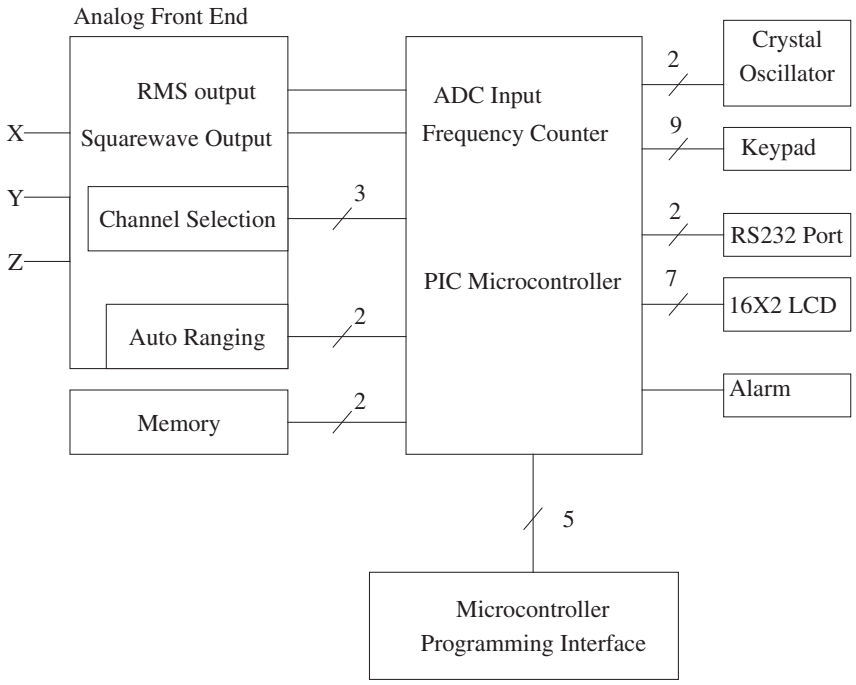

Fig. 3. Top hierarchy model design for the isotropic Gaussmeter IDR-200.

Fig. 4. Front panel for the Gaussmeter IDR-200.

components of the meter to operate from 0 to 50° C, and all the critical gain stages are based on resistor ratios, which should remain constant as temperature varies.

5.2. Measurement results

The measurements were carried out at least 1 m above-ground using the three-dimensional isotropic probe with frequency indicator to ensure omnidirectional measurements. Depending on the environments, the overall campaign consisted of either spot or long-term measurements that are adjusted by using the timer-controlled recording function. These values can then be output in a file via a PC fitted with appropriate software.

5.3. Electromagnetic field emission from video display terminals

Video display terminals have been commonly used along with flat screen monitors for displaying information for a system like a computer and keyboard. A VDT produces low levels of electromagnetic (EM) field because of the techniques used to generate and move the electron beam that illuminates the screen of a cathode ray tube (CRT). The EM field generated by a VDT extends over a broad spectrum, including VLF frequency and low frequency energy (30–300 kHz). These displays are also used in television receivers, automated teller machines, video games, and other devices.

Measurements performed around a VDT show the electromagnetic fields are confined to the conductors and no significant electromagnetic wave radiation traveling away from the CRTs has been detected [8]. So we can correctly talk of magnetic fields associated with either conductors or coils passing right through the body without any appreciable attenuation but ironically have been found to have many significant biological effects [20]. Furthermore the electric field originates from the surface of the CRT screen and terminates on the skin of the human operator [21].

A CRT is an evacuated glass tube, which consists of several basic components, as illustrated in Fig. 5. The electron gun generates a narrow beam of electrons. The anodes accelerate the electrons. Deflecting coils produce the low frequency electromagnetic fields that allow for constant adjustment of the direction of the electron beam. There

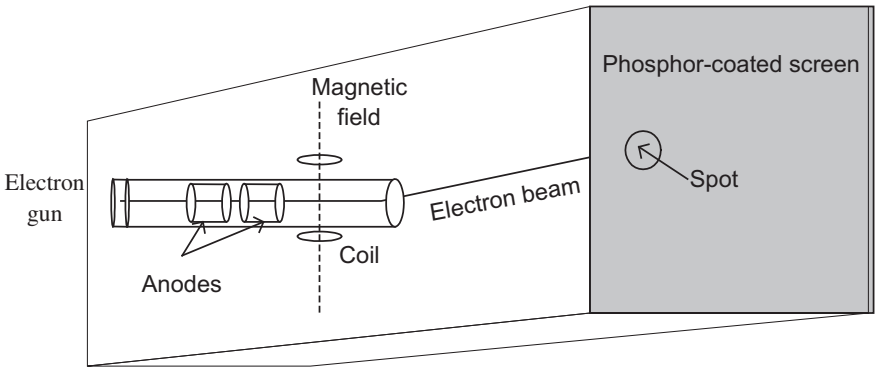

Fig. 5. Drawing model of a CRT.

are two sets of deflecting coils: horizontal and vertical. Only one set of coils is shown for simplicity in Fig. 5. The intensity of the beam can vary. The electron beam produces a tiny, bright visible spot when it strikes the phosphor-coated screen. Only one electron gun, which is typical of a monochrome CRT, is shown in Fig. 5.

Most modern CRTs render color images. These devices have three electrons guns, one for each of the primary colors: red, green, and blue. This type of CRT is called an RGB color monitor and produces three overlapping images: one in red, one in green and one in blue. The electron beam in the CRT moves across the screen in a series of horizontal and vertical lines. For each horizontal line, the beam must be swept constantly across the screen by an increasing magnetic field while the electron beam is turned on. Once the beam reaches the right-hand edge of the screen, the electron beam is turned off and retraced to the left side of the screen by a rapidly decreasing magnetic field. The phenomenon of slow and fast changing magnetic fields produces a sawtooth-shaped waveform as shown in Fig. 6. This horizontal deflection fringing magnetic field at the VDT for the model Magnavox CM8762 was captured by using the analog output of the VLF Gaussmeter. Based on the simplified block diagram of the measurement system as shown in Fig. 2, the analog output is able to display the original waveforms from 1 kHz to 200 kHz after filtration, integration, and amplification for periodic or non-periodic waves induced by the three-axis air coil. The magnetic flux density of the 60 Hz fringing waveform field for the vertical deflection close to the VDT screen is shown

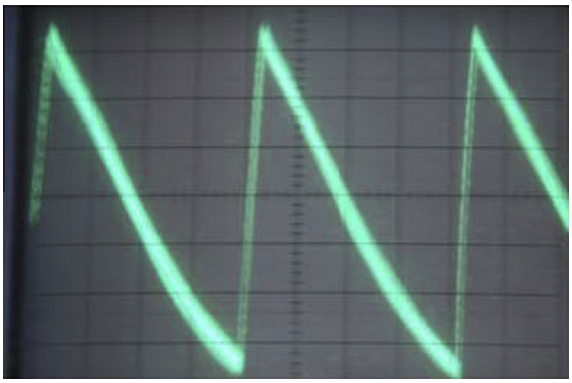

Fig. 6. Sawtooth waveform (horizontal deflection) at frequency of 16 kHz captured close to VDT screen model Magnavox CM8762 with (0.2 V/div.).

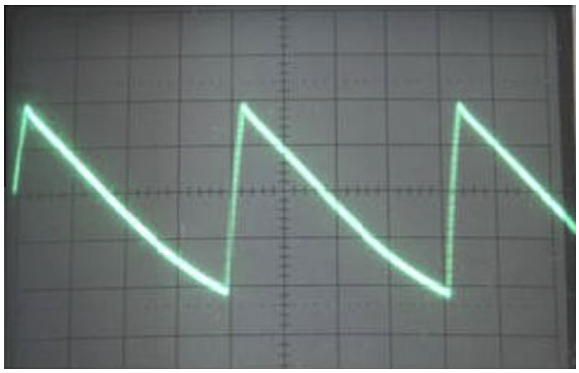

Fig. 7. Periodical waveform (vertical deflection) with frequency of 60 Hz captured close to VDT screen model Magnavox CM8762 (0.1 V/div.).

in Fig. 7. This waveform voltage was measured at the analog output of the three-axis ELF Milligaussmeter model IDR-210. This device has the BW limitation between 20 Hz and 4 kHz.

The horizontal deflection system operates at frequency of 15–100 kHz, and is the major source of VLF electric and magnetic fields in the VDT. While the vertical deflection system operates at a frequency of 50–80 Hz in the majority of VDTs, and is the major source of SLF fields. In computer systems, there are several displays modes, such as monochrome, and technologies known by the acronyms such as CGA, EGA, VGA and SVGA. The field strengths emanating from different units vary with the product design.

The VLF magnetic field BR around an SVGA monitor made by Magnavox model CM2089 located at our facility was mapped from four different positions by using the Gaussmeter IDR-200: the left, right, rear, and front of the VDT. This particular monitor was selected randomly from the monitors located inside our lab. For each of the four positions, the magnetic field was measured at fixed points on a plane through the x and y coordinates with dimensions 38×38 cm as shown in the bottom left or right of Figs. 8–11. The spacing between each measurement point on each axis is 7.62 cm, and 36 points were recorded for each side. For each side of the VDT, the height of the x–y measurement plane was selected by finding the highest magnetic field. The x-axis is parallel and very close to the housing of the VDT while the y-axis direction is perpendicular to the enclosure of the monitor.

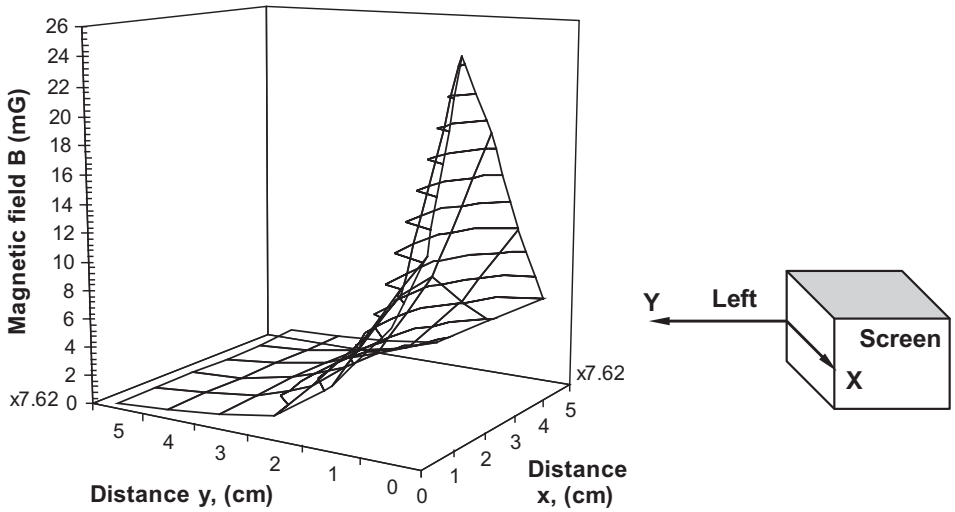

Fig. 8. Mapping of magnetic flux density B_R horizontal deflection field at the left side of the VDT with $f = 31$ kHz.

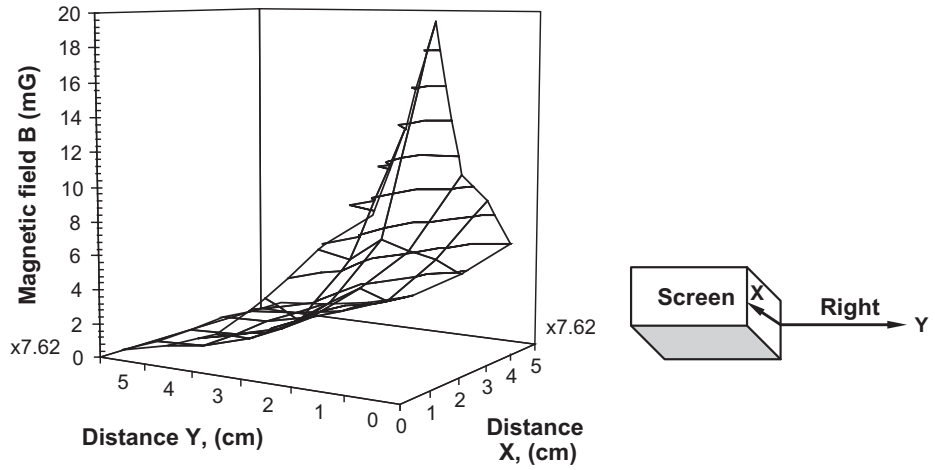

Fig. 9. Mapping of magnetic flux density B_R horizontal deflection field at the right side of the VDT with $f = 31$ kHz.

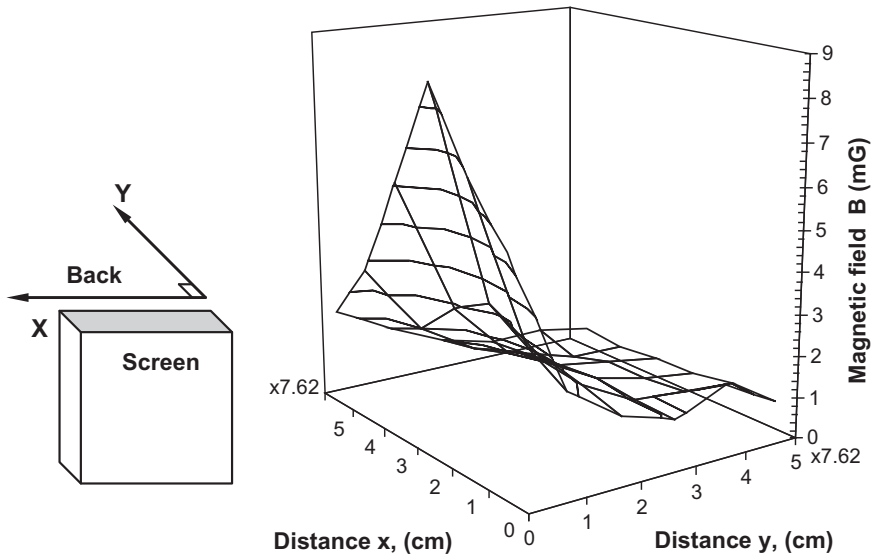

Fig. 10. Mapping of magnetic flux density B_R horizontal deflection field at the backside of the VDT with $f = 31$ kHz.

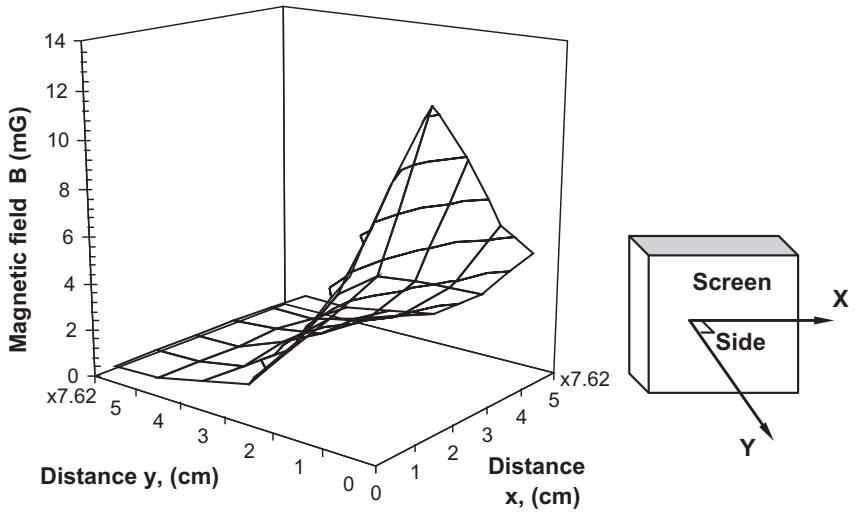

Fig. 11. Mapping of magnetic flux density B_R horizontal deflection field at the screen side of the VDT with $f = 31$ kHz.

The map of the magnetic field for the horizontal deflection at the left side of the VDT is shown in the bottom left of Fig. 8. The peak value $B_R = 24.6$ mG is located at the grid point $x = 2$ and $y = 0$. It can be seen that the magnetic field readings are higher near the source coil or conductors, and they fall off very rapidly while moving away from the source. The magnetic fields generated by a multiple conductor source usually decrease at a nonlinear rate of $1/(y^2)$ as the distance y from the VDT increases [8]. The frequency measured by the VLF Gaussmeter for the horizontal deflection was 31 kHz.

The procedure measurement of the magnetic field for the horizontal deflection at the right side of the VDT is shown in the bottom right of Fig. 9. The maximum reading B_R is 19.6 mG on the right side of the VDT is located at the grid point $x = 2$ and $y = 0$ with frequency $f = 31$ kHz as illustrated by Fig. 9.

The VLF magnetic on the sides and to the rear falls so rapidly that people located in those directions receive only a small fraction of the exposure.

The maximum reading B_R is 8.6 mG on the rear of the VDT is located at the grid point $x = 2$ and $y = 0$ with frequency $f = 31$ kHz as illustrated by Fig. 10.

The important locations where the SLF and the VLF magnetic field need to be checked are in the front of the screen where the operator may be exposed. The maximum reading B_R horizontal is 12.4 mG on the front of the VDT is located at the grid point $x = 2$ and $y = 0$ with frequency $f = 31$ kHz as shown by Fig. 11.

The maximum reading B_R vertical is 10.4 mG on the front of the VDT is located at the grid point $x = 2$ and $y = 0$ with frequency $f = 60$ Hz as shown by Fig. 12. The 60 Hz sinusoidal fields are generated mainly from power transformer.

More measurements of the magnetic flux densities with frequencies are taken for various CRT displays at certain distances. These data are given in Tables 3 and 4. The measurement points for each device were selected at the highest field levels on the front surface and moving away from the front of the devices in a straight line perpendicular to the surface. The distance of 15 cm from the VDT is approximately over a keyboard, and the distance of 50 cm is about the position of the user. The comparison results from Tables 3 and 4 to ICNIRP reference levels for occupational and general public exposure (Tables 1 and 2) show all the measured values of the magnetic fields for different frequencies are below the reference levels.

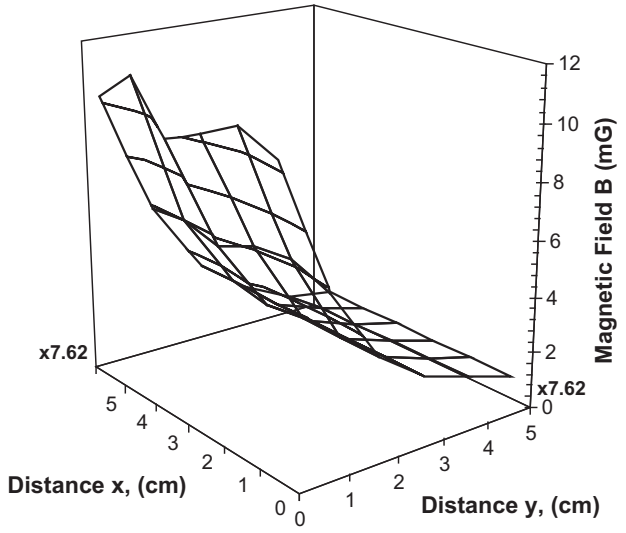

Fig. 12. Magnetic flux density distribution B_R for vertical deflection field at the front side of the VDT with $f = 60$ Hz.

It is true that soon, LCD flat screen display monitors will replace the most VDTs in the market. However, VDTs are still better than LCDs for some applications that require very high resolution or high color accuracy, such as medical imaging, and VDTs will continue to be used for these applications in the future. There is also a large number of VDTs, such as televisions and computer monitors, currently in use that will not be replaced by LCDs for many years. Since VDTs were so widely used, this paper will be very beneficial for historical cancer epidemiological studies worldwide among workers who used the VDT in their jobs for many years.

Table 3
RMS Measurement of magnetic flux density B_R (mG) and frequency horizontal deflection fringing field at different distances from the fronts of the CRTs.

CRT model	0 (cm)	15 (cm)	30 (cm)	50 (cm)	Frequency (kHz)
Hp pavilion mx75	3.8	1.0	0.6	0.4	39
Magnavox CM8762	17.1	4.6	1.6	0.8	16
Magnavox CM2089	12.4	3.1	1.1	0.8	31
Sony Trinitron color TV, kV-27V10	22.5	5.6	2.5	1.2	16
Sharp TV 32U-S50	8.5	4.4	1.3	0.8	17
Dell Trinitron Ultrascan P991	10	1.6	1.0	0.6	60
RCA T09085	15	4.6	5.4	4.4	73
Compaq CV715	4.8	1.4	1	0.9	60

Table 4
RMS measurement of magnetic flux density B_R (mG) vertical deflection at 60 Hz fringing field at different distances from the fronts of the CRTs.

CRT model	0 (cm)	15 (cm)	30 (cm)	50 (cm)	Frequency (Hz)
Hp pavilion mx75	8.4	1.7	0.8	0.2	60
Magnavox CM8762	30.6	8.2	3.0	1.3	60
Magnavox CM2089	11.4	3.36	1.6	0.34	60
Sony Trinitron color TV, kV-27V10	35	10.6	4.6	3.0	60
Sharp TV 32U-S50	23	10.5	4.4	2.1	60
Dell Trinitron Ultrascan P991	6.3	2.2	1.4	0.4	75
RCA T09085	23.4	7.7	4.7	1.6	60
Compaq CV715	5	1.4	0.4	0.2	75

5.4. Induction heating process

Induction heating is a method of providing fast and consistent heat for manufacturing applications that involve changing the properties of metals or other electrically conductive materials. The process relies on induced electrical currents within the material to produce heat [22].

The basic components of an induction heating system are an AC power supply, induction coil, and material to be heated. High frequency currents typically in the kHz are passed through coils that surround the conductive materials to be heated or treated. Strong eddy currents are produced in the target material generating large amounts of heat without any physical contact between the coil and the material. There is a relationship between the frequency of the alternating current and the depth to which the magnetic field penetrates the work pieces; low frequencies of 5–30 kHz are effective for thicker materials requiring deep heat penetration, while higher frequencies of 100–400 kHz are effective for smaller parts or shallow penetration. The illustration of an induction heater is shown in Fig. 13. Shown is a Radyne VersaPower current source induction heating system, which includes a Flexitune 30 kW power supply made by Radyne, Milwaukee, WI, a heating coil, and a heat load made from steel billet. The heating coil has 3 turns of ¼″ tubing with a 3½″ inside diameter, and the heat load has a diameter of 2″ and is 6″ long. The Gaussmeter model #: IDR-200 was used to measure the magnetic field and the frequency for this system

Fig. 13. Measuring setup where the three-axis coils of the VLF Gaussmeter are placed nearby the heat load and the coil connected to the Flexitune 30 kW power supply made by Radyne. (Photo courtesy of the Radyne Corporation of America, Milwaukee, WI).

Table 5
RMS magnetic flux density values are taken at different distances between the induction heater and sensor at 25 kHz and 24.5 kW.

Distance from the induction heater (cm)	B_R (μT)
20	154.86
30	37.12
40	17.95
50	8.76
60	4.40
70	2.88

for the three axes at each measurement point. The data given in Table 5 show how the magnetic field strength around the conductive material decreases with distance from the source, which was at a steady state in the heating process. By comparing these results to the ICNIRP reference levels for occupational and general public exposure (Tables 1 and 2), we noticed at 20 cm the measured magnetic field was higher than the reference level, and the rest of the results are acceptable.

Although magnetic fields are the most prominent feature of the induction heating process, a strong magnetic field is required for changing the physical structure of the material, the stray magnetic field in the vicinity of the coils may exceed the applicable exposure limits in some cases. People with implanted ferromagnetic or electronic medical devices can suffer from interferences with magnetic field above certain level. This induction heating process is also used inside some household appliances like the electric stove. Some simple precautions should be followed, such as using the Gaussmeter to measure the magnetic field around the system and determine the safest spot for the person to stand while the induction heating system is active.

5.5. Hybrid cars

Gas-electric hybrid cars are poised to become the most popular design of vehicles for passengers. Without a doubt, scientists and consumers agree that hybrid vehicles are

cleaner for the planet and more economical due to the reduced fuel consumption. However, there is another more immediate concern: Are hybrids healthy for drivers? This question was addressed in the New York Times [23]. In addition to that, the end-users have the right to know whether or not the magnetic field emitted from these cars imposes a health hazard. One concern with hybrid vehicles is that the flow of AC and DC electrical currents inside the automotive components can be much larger than standard gas powered vehicles and can produce larger magnetic fields.

The main components of the new electric drive train are the electric motor, the power converter, the power supply, and the wires connecting these components [24]. Each of them is a source of electromagnetic field (EMF) emissions. The power converter is especially known as the main source of EMF emissions. Fig. 14 represents the basic elements for a standard hybrid car; it also shows the bi-directional path of the DC current between the electric motor and the battery charger. This circulation of current will develop a static magnetic field around the conductor located along the floor of the car.

To address these concerns, we decided to do our own measurements for some hybrid and gasoline cars by using three different kinds of Gaussmeters made by Integrity Design & Research Corporation. For more accuracy on the testing, it is impossible to have one single model of Gaussmeter to do all the measurements from static to VLF frequency at different sensitivities.

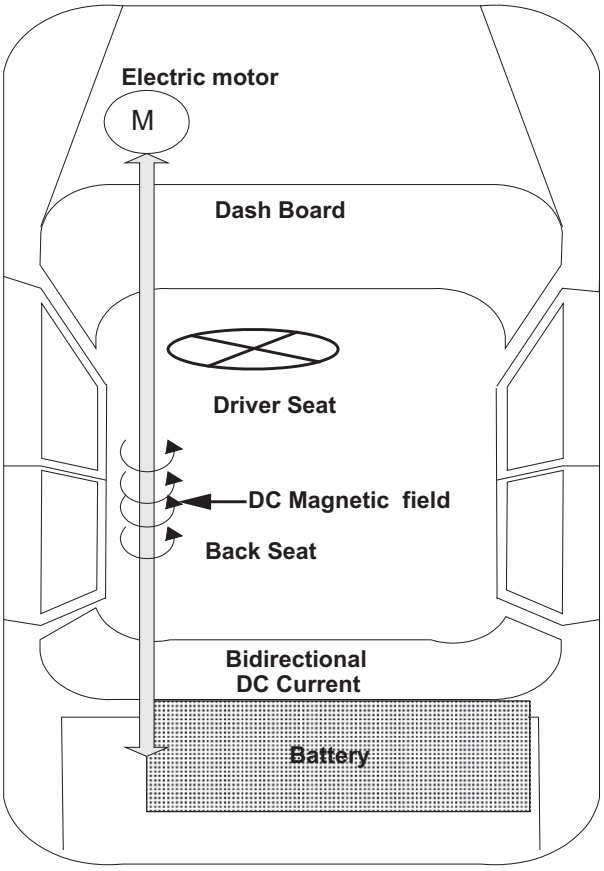

Fig. 14. Some components of interests for a hybrid car are under testing for magnetic fields.

Since the battery is mounted in the back of hybrid cars and the power cables must connect the battery to the front components, they are often placed underneath the driver and rear side. Therefore, some exposure to DC magnetic fields is unavoidable due to the flow of a DC current inside the cables. For this task, we used a DC Gaussmeter model IDR-309-T with a transverse hall probe and a resolution of 1 mG. This meter measured only the static magnetic field. For the AC magnetic field measurements, we, first, used the Gaussmeter IDR-200 for frequencies above 4 kHz, and, second, the Gaussmeter model IDR-210. The latter is an isotropic meter with a bandwidth of 20 Hz–4 kHz and resolution of 0.2 mG at 200 mG scale.

The measurements were done when the cars were running at different speeds and when they were parked. The testing results were not simple or straightforward, because the EMF kept changing, depending on the engagement mode of the cars. Acceleration, deceleration, breaking, air conditioning, external EMF atmosphere, and other factors all directly affect the EMF emissions. The results of this testing were only approximate at best. The AC magnetic field measurements were the most reliable comparing to the DC ones.

The DC magnetic tests were not feasible with the vehicle in motion through the earth's magnetic field that varies with the maximum value close to 550 mG in the northern part of the USA, even with no other vehicles in the vicinity. Before taking the static measurement, we zero out the meter IDR-309-T from any external magnetic field interference by inserting the hall probe inside a zero gauss chamber. The highest reading was close to 2 G at the floor level when the electric motor is running. The reading diminished upward to about 2 mG at the driver seat and 10 mG at the rear seat.

For VLF magnetic fields, there was a regular fluctuation below 2 mG when the operating electric motor is running alone. The frequencies registered on the meter model IDR-210 were mainly the first, second, and third harmonics of 60 Hz. Sometimes higher frequencies up to 2 kHz were noted. Also, we noted sometimes that the AC magnetic fields were consistently higher on the rear seat than the front ones. Table 6 shows the maximum AC magnetic field measurements for some hybrid and standard vehicles.

Table 6
Magnetic field ranges inside the hybrid and gasoline cars are measured by IDR-210.

Car's model	Dashboard	Driver seat	Rear driver seat	Passenger seat
Maximum RMS magnetic flux density values B_R (mG)				
Toyota prius hybrid 07	35	10	6	2
Toyota prius electric 07	30	8	5	2
Ford escape 06 hybrid	5	5	20	1
GM lumina 97 gasoline	1.5	0.8	0.5	0.2
Toyota highlander 2008 hybrid	2.8	1.4	5.4	2.6
Dodge durango 2000 gasoline	5.2	2.2	1.8	0.2

These measurements were obtained by using the Gaussmeter IDR-210.

After providing this data on some hybrid car models, it is obvious that these measurements did not meet the Swedish MPR-II standard for ELF magnetic fields [26] or to the NY state power lines project final report [27]. Both standards stated that levels higher than 2–3 mG correlate to twice the cancer risk for people exposed to the magnetic fields at super and ultra low frequency. But these data meet the ICNIRP's safe exposure level mentioned in the introduction.

6. Conclusions

This paper reports the results of magnetic field measurements in the near field region using complementary Gaussmeters to better understand the nature of the magnetic fields. We explicitly mapped and studied the frequencies and magnetic fields around different kinds of VDTs, around one model of an induction-heating unit, and finally inside different models of gas and electric cars. The measurements were made to determine whether internationally accepted reference levels and other standards like the Swedish standard for safe exposure were violated, especially around the VDT. The magnitudes of the measured field values were within the recognized guidelines based on the ICNIRP standard, suggesting that the fields are not dangerous and there is therefore no cause for concern among the public or working personnel for the selected case studies. However, the general public should always evaluate new technologies that use magnetic energy, such as, the Duracell "myGrid" and the WiTricity power distribution technology, before wide scale adoption.

Despite these scientific findings, the duration of exposures in many studies has been brief compared to typical occupational exposure time over a career, a typical lifespan, or latency periods for diseases such as cancer. Until very recently no large scale epidemiological studies on CRT users have been completed. Unfortunately, some of the measurements taken above did not meet the Swedish standard stating that the levels higher than 2–3 mG correlated to twice the cancer risk for people exposed to the magnetic fields. This conflict reveals the need for a conclusive solution to settle this matter once and for all.

References

[1] R.O. Becker, Cross Currents, Penguin Putnam, New York, 1990. pp. 173–304.

[2] A.S. Safigianni, C.G. Tsompanidou, Measurements of electric and magnetic fields due to the operation of indoor power distribution substations, IEEE Trans. Power Del. 20 (3) (2005) 1800–1801.

[3] Possible health hazards from exposure to power–frequency electric and magnetic fields – a COMAR technical information statement, IEEE Eng. Med. Biol. 19(1) (2000) 131–137.

[4] International Commission of Non Ionizing Radiation Protection (ICNIRP), Guidelines for limiting exposure to time-varying electric and magnetic fields (1 Hz to 100 kHz), Health Phys. 99(6) (2010) 818–836.

[5] N. Wertheimer, E. Leeper, Electrical wiring configurations and childhood cancer, Am. J. Epidemiol. 109 (3) (1979) 273–284.

[6] C.A.L. Bassett, Pulsing electromagnetic fields: a new method to modify cell behavior in calcified and noncalcified tissues, Calcif. Tissue Int. 34 (1) (1982) 1–8.

[7] A. Libbof, Time-varying magnetic field: effect on DNA synthesis, Science 223 (4638) (1984) 818–820.

[8] R. Habash, Electromagnetic Fields and Radiation: Human Bioeffects and Safety, Marcel Dekker, New York, 2001. pp. 65–123.

[9] L. Tomenius, 50-Hz electromagnetic environment and the incidence of childhood tumors in Stockholm county, Bioelectromagnetics 7 (2) (1986) 191–208.

[10] R.J. Spiegel et al., Measurement of small mechanical vibrations of brain tissue exposed to extremely-low-frequency electric fields, Bioelectromagnetics 7 (3) (1986) 295–306.

[11] N. Wertheimer, E. Leeper, Possible effects of electric blankets and heated waterbeds on fetal development, Bioelectromagnetics 7 (1) (1986) 13–22.

[12] F.S. Barnes, Mechanisms for electric and magnetic fields effects on biological cells, IEEE Trans. Magn. 41 (11) (2005) 4219–4224.

[13] M.E. Herniter, Schematic Capture with Cadence PSpice, second ed., Prentice Hall, Upper Saddle River, NJ, 2003. pp. 54–428.

[14] C.C. Lo, T.Y. Fujita, A.B. Geyer, T.S. Tenforde, A wide range portable 60-HZ magnetic dosimeter with data acquisition capabilities, IEEE Trans. Nucl. Sci. 33 (1) (1986) 643–646.

[15] T.L. Floyd, Electronics Fundamentals Circuits, Devices, and Applications, fifth ed., Prentice-Hall, Upper Saddle River, NJ, 2001. pp. 612–631.

[16] S. Hanna, W. Varhue, Y. Motai, S. Titcomb, Very-low-frequency electromagnetic field detector with data acquisition, IEEE Trans. Instrum. Meas. 58 (1) (2008) 129–140.

[17] G. Crotti, Domenico Giordano, Evaluation of frequency behavior of coils for reference magnetic generation, IEEE Trans. Instrum. Meas. 54 (2) (2005) 718–721.

[18] O. Bottauscio, G. Crotti, S. D'Emilio, G. Farina, A. Mantini, Generation of reference electric and magnetic fields for calibration of power-frequency field meters, IEEE Trans. Instrum. Meas. 42 (2) (1993) 549–552.

[19] EPA, Laboratory testing of commercially available power frequency magnetic field survey meters, June 1992, pp. 3–4.

[20] W.T. Kaune, Coupling of Living Organisms to ELF Electric and Magnetic Fields. Biological and Human Health Effects Of Extremely Low Frequency Electromagnetic Fields, American Institute of Biological Sciences, Arlington, VA, 1985.

[21] D. Sapashe, J.R. Ashley, Video display terminal fringing magnetic field measurements, IEEE Trans. Instrum. Meas. 41 (2) (1992) 178–184.

[22] Y. Ge, R. Hu, Z. Zhang, Q. Shen, Optimization Control of Induction hardening Process, IEEE Int. Conf. Mechatr. Autom., June 2006, p. 1126.

[23] J. Motavalli, Fear, but few facts, on Hybrid risk, 27 April, 2008. <http://www.nytimes.com/2008/04/27/automobiles/27EMF.html>.

[24] S. Guttowski, S. Weber, E. Hoene, W. John, H. Reichi, EMC issues in cars with electric drives, in: 2003 IEEE International Symposium on Electromagnetic Compatibility, pp 777–782.

[25] R. Sekerinska and V. Dimcev, Measurement of power frequency magnetic fields in different environments, in: IEEE 10th Mediterranean Electrotechnical Conference, vol. III, 2000, pp. 1107–1110.

[26] User's Handbook for Evaluating Visual Display Units, Technical Report MPR, 1990.

[27] A. Ahlbom et al., Biological effects of power line fields, New York state power lines project scientific advisory panel final report, July 1987.